A NON-ISOTROPIC MULTIPLE-SCALE TURBULENCE MODEL

Contract No. NAS8-36955 D.O.31

Final Report

Period of Performance
March 15, 1989 - September 15, 1990

by
C. P. Chen

Department of Chemical Engineering
The University of Alabama in Huntsvilie
Huntsville, AL 35899

for

National Aeronautics and Space Administration
George C. Marshall Space Flight Center
Marshall Space Flight Center, AL 35812

CONTENT

LIST OF TABLES

LIST OF FIGURES

ABSTRACT

This report describes a newly developed non-isotropic multiple-scale turbulence model (MS/ASM) for complex flow calculations. This model focuses on the direct modeling of Reynolds Stresses and utilizes split-spectrum concepts for modeling multiple-scale effects in turbulence. Validation studies on free shear flows, rotating flows and recirculating flows show that the current model perform significantly better than the single-scale $k-\epsilon$ model. The present model is relatively inexpensive in terms of CPU time which makes it suitable for broad engineering flow applications.

INTRODUCTION

Presently the great majority of engineering flow computations are based on an eddy viscosity linkage through Reynolds-stresses/Mean-strain rate constitutive relationship, the most often used version being one in which the eddy viscosity is obtained from local values of the turbulence kinetic energy (k) and its dissipation rate (ϵ) [1]. The k and ϵ are obtained from transport differential equations solved simultaneously with the mean momentum equations. Some of the shortcomings inherent in this type of $k-\epsilon$ models are : (a) the use of one set of characteristic scales to represent a spectrum of eddy sizes and, (b) the isotropic assumption of the gradient type eddy viscosity Reynolds-stress/strain rate constitutive formulation. Experimental observations indicate that energy-containing, turbulence generating eddies are larger and exhibit a different rate of development than do smaller turbulence energy dissipating eddies. In the classical turbulence models such as the $k-\epsilon$ model and the Reynolds stress models [2], only the generation and dissipation of turbulent kinetic energy are considered while the cascading processes are assumed to be in equilibrium.

Besides, the effect of rotation on the turbulence, especially through the modification of the turbulent energy cascading process, has not been explored by the conventional single-scale models. Experimental data shows that the predominant effect of rotation is

to decrease the rate of dissipation of the turbulence and increase the lengthscales, especially those along the axis of rotation. Due to the generation of inertial waves, the net energy transfer from large eddies to small ones was reduced. To account for the different mechanisms involved in the evolutions of different eddies, the generation, cascade, and dissipation of turbulent kinetic energy have to be considered.

In this study, we have developed a multiple-scale turbulence model based on the split-spectrum methodology of Hanjalic et al [3]. This model is derived by partitioning the turbulent kinetic energy spectrum into a set of wave number regions, by integrating the partitioned energy spectral density equation to obtain the energy evolution for each wave number region, and by considering the energy transfer rate between the adjacent wave number regions. Recent developments including the rotation effect and anisotropy effect will be described. Model validations including homogenous rotating flows, free shear flows and recirculating flows will be compared with available experimental data and other single-scale turbulence models.

THE TURBULENCE MODEL

The underlying idea of the multiple-scale model has been described in [3,4]. To summarize, the closures and the convection-diffusion equations for the model are described below. The turbulent kinetic energy and the energy transfer rate equations for the energy-containing large eddies are given as

$$\frac{\partial k_p}{\partial t} + U_j \frac{\partial k_p}{\partial x_j} = \frac{\partial}{\partial x_j}\left(\frac{\nu_t}{\delta_{k_p}} \frac{\partial k_p}{\partial x_j}\right) + P_r - \epsilon_p \tag{1}$$

$$\frac{\partial \epsilon_p}{\partial t} + U_j \frac{\partial \epsilon_p}{\partial x_j} = \frac{\partial}{\partial x_j}\left(\frac{\nu_t}{\delta_{\epsilon_p}} \frac{\partial \epsilon_p}{\partial x_j}\right) + C_{p_1} \frac{P_r \epsilon_p}{k_p} - C_{p_2} \frac{\epsilon_p^2}{k_p} - C_{p_3} \Omega \epsilon_p \tag{2}$$

where P_r is the energy production rate represented by $P_r = -\overline{u_i u_j} \partial U_i / \partial x_j$. The turbulent kinetic energy equation and the dissipation rate equation for the fine scale eddies are given as

$$\frac{\partial k_t}{\partial t} + U_j \frac{\partial k_t}{\partial x_j} = \frac{\partial}{\partial x_j}\left(\frac{\nu_t}{\delta_{k_t}} \frac{\partial k_t}{\partial x_j}\right) + \epsilon_p - \epsilon_t \tag{4}$$

$$\frac{\partial \epsilon_t}{\partial t} + U_j \frac{\partial \epsilon_t}{\partial x_j} = \frac{\partial}{\partial x_j}\left(\frac{\nu_t}{\delta_{\epsilon_t}} \frac{\partial \epsilon_t}{\partial x_j}\right) + C_{t_1} \frac{\epsilon_p \epsilon_t}{k_t} - C_{t_2} \frac{\epsilon_t^2}{k_t} - C_{t_3} \Omega \epsilon_t \tag{5}$$

In the above equation, Ω is the local mean vorticity or angular velocity of the rotating frame. The model constants in equations (1) - (4) have been determined by transforming the modeled turbulence equations into asymptotic turbulence decay rate equations of grid-generated homogeneous turbulence and other simplified flow situations. Detailed derivation of the system of equations for the model constants which is similar to that in Ref. [4] can be found in Appendix A. These model constants are given in Table 1.

If the above turbulence model equations are used to construct an eddy viscosity based on Boussinesq assumption, the eddy viscosity formula proposed here is given as

$$\nu_t = C_\mu \frac{(k_p + k_t)^2}{\epsilon_p} \tag{6}$$

and the Reynolds stress tensor is expressed as

$$\overline{u_i u_j} \equiv R_{ij} = -\nu_t S_{ij} + \frac{2}{3} \delta_{ij} k \tag{7}$$

in which

$$S_{ij} = \frac{1}{2}\left(\frac{\partial U_i}{\partial x_j} + \frac{\partial U_j}{\partial x_i}\right) \tag{8}$$

$$k = \frac{1}{2} \overline{u_i u_i} \tag{9}$$

As discussed widely in the literature, the linear isotropic constitutive relationship used in equation (7) yields highly inaccurate predictions for the normal Reynolds stress differences. For example, in a fully developed turbulent channel flow, equation (7) predicts that the normal Reynolds stresses are all equal, i.e., that

$$R_{11} = R_{22} = R_{33} \quad (\overline{u_1 u_1} = \overline{u_2 u_2} = \overline{u_3 u_3})$$

which indicates isotropic turbulence and is in contradiction to experimental observation. In this study, the non-isotropic aspect of the turbulence will be modeled based on simplification of the second-moment closure methodologies. In the second-moment closure, the

transport equation for Reynolds stress components R_{ij} was derived [5,6] :

$$\frac{D}{Dt}(\rho R_{ij}) - D_{ij} = P_{ij} + \Phi_{ij} - \epsilon_{ij} \tag{10}$$

in which the terms on the left hand side of (10) represent the convective and diffusive transport of R_{ij}, respectively, and the terms on the right hand side represent the production, pressure-strain (redistribution), and viscous dissipation tensors of Reynolds stress. Among these terms, closure assumptions are required for D_{ij}, Φ_{ij} and ϵ_{ij}. To date, equation (10) still represents the most complex turbulence models used in engineering calculations for which the non-isotropy and extra complex strains can be automatically accounted for. However, the extra Reynolds stress differential transport partial differential equations (six of them for 3-D flows) required to be solved introduce severe computer cost penalty. As a result, the approach used in this study to retain the advantages of this level of modeling is to simplify the differential transport equations such that they reduce to algebraic expressions, the so called Algebraic Stress Model (ASM)[7].

There are several approaches for algebraic stress model formulations. The one adopted here is the similitude analysis proposed by Mellor and Yamada [8]. Their formulation leads to linear algebraic equations for the stresses based on a rigorous similitude analysis of the transport equation for anisotropy ($\overline{u_i u_j} - 2/3\delta_{ij}k$). This approach does not subject to the limitation that $\overline{u_i u_j}/k$ = constant assumption invoked by Rodi [2]. Equation (10) was thus simplified to :

$$P_{ij} - \frac{2}{3}\delta_{ij}P_k + \Phi_{ij} \cong 0 \tag{11}$$

It should be noted that the model for Φ_{ij} should be consistent with the order of magnitude analysis which leads to equation (11). The model proposed in this study has the following form :

$$\Phi_{ij} = -c_1\rho\frac{\epsilon_t}{k_t}(\overline{u_i u_j} - \frac{2}{3}\delta_{ij}(k_p + k_t)) - c_2(P_{ij} - \frac{2}{3}\delta_{ij}P_k) \tag{12}$$

and

$$P_{ij} = \overline{u_i u_j}\frac{\partial U_i}{\partial x_j} \tag{13}$$

$$P_k = \frac{1}{2} P_{ii} \tag{14}$$

The first term on the right hand side of equation (12) contains only turbulent velocities and is formulated after Rotta's linear return-to-isotropy model [6]. Note that the time scale used in the turbulence time scale associated with the high frequency eddies in the multiple-scale model. Detailed derivations can be found in Appendix B. The above model causes a tendency towards isotropy if c_1 is greater than unity. In this study, c_1 is chosen to be 1.8 - 0.5 f in which f is a wall correction term affecting the normal redistribution actions of the pressure-strain correlation. This "echo" effect has been discussed extensively in the literature [5,6]. We use the following simple proximation function :

$$f = 1 - (\frac{y}{D})^2$$

where y is the distance from wall and D is the half width of the duct passage.

The second term on the right hand side of equation (12) is referred to as the "mean-strain" part of the pressure-strain tensor. We model this term based on the "isotropization of production" of Ref. [5]. As seen from the formulation, this term associates with the production of turbulent kinetic energy and thus links with the time scale of the energy containing eddies. The constant used here is $c_2 = 0.85 - 0.06f$.

For wall bounded flows, a ratio of k_t/k_p was derived based on the wall function approach [2]. For practical purposes, these wall functions were derived from the near-wall equilibrium assumptions and logarithmic velocity profiles. Detailed derivations and formulations can be found in Appendix C.

RESULTS AND DISCUSSIONS

For model validations, several testing cases including grid-generated turbulence with rotation, free shear flows and two-dimensional as well as axi-symmetric recirculating flows are calculated.

Grid-Generated Rotating Flows

The structure of the turbulence is changed through the action of the Coriolis forces : the turbulent length scales are increased in the rotation axis and the energy cascading from larger toward smaller dissipative eddies is inhibited [9]. Figure 1 compares the numerical predictions of the multiple-scale model with corresponding experimental conditions of Wigland and Nagib [10] as listed in Table 2. The model provides quite accurate predictions of the decay of turbulence intensity at different rotation rates and different flow conditions. The agreement is good for all cases, even when in case (2) the turbulence decays faster for $\Omega = 20s^{-1}$ due to different initial time scales. Under the same initial conditions, the model predicts slower decay of the turbulence with increasing rates of rotation, in agreement with the data. It should be noted that the standard $k - \epsilon$ model is insensitive to changes in rotation rates because it has no provision to account for this effect.

Free Shear Flows - Jets

The necessary step in turbulence model development is to use the model to predict free shear flows. Here, three different jet flows in the fully developed region (self-similar regions) are calculated using an accurate finite different scheme based on Keller's Box method. The set of governing partial differential equations were transformed to a set of coupled ordinary differential equations. Such as the final coupled ordinary differential equations for the round jet is shown in Appendix D. Details of the numerical scheme and the method of calculating sharp boundaries between turbulent shear flows and irrotational ambient fluid can be found in [11]. The multiple-scale model used here is the one associated with an eddy viscosity formulation of equation (6) (the MS/EV model).

The computed values of the spreading rates of the plane jet, round jet and radial jet using the MS/EV model are given in Table 3. Also shown for comparison are the computed spreading rate using various single-scale models as well as the experimental values for these quantities. The spreading rate of the round jet is experimentally observed to be about 20

% less than that of the plane jet. The inclusion of the rotation time scale in the MS/EV model has the effect of increasing the energy transfer rate from energy-containing eddies down to the dissipative eddies due to the vortex stretching mechanism and produced less spreading for the round jet. The MS/EV model gives the best overall predictions in terms of spreading rate for these jet flows.

In Figure 2-4, the dimensionless mean velocity of the three jets are plotted versus the similarity coordinates in which the transverse locations are normalized with the velocity half-width. The mean velocities calculated using various models are all in reasonable agreement with the data over the central position of the jet but deviates towards the edge of the jets. This is due to the intermittence close to the free turbulent/non-turbulent interface and the turbulence models do not model these unsteadiness explicitly. The MS/EV model appears to give better predictions than the others and gives a little wider jets.

2D Backward-Facing Step Flow

For this and the following case, the governing partial differential equations were solved in the fully elliptic form. The differential equations were discretized based on the control-volume approach with a non-staggered grid arrangement. A second order upwind differencing scheme is employed for convection terms. A time-marching sequence employs the PISO[12] algorithm to resolve the momentum equation using the pressure incremental equation which enforces continuity at each time step. Calculations are carried out until steady state solutions are reached. Details of the numerical method can be found in [13].

The predicted values of the reattachment length of the recirculation zone behind the step were made using the standard $k-\epsilon$ model, the single- scale Algebraic Stress Model ($k-\epsilon$ / ASM), the multiple-scale model with eddy viscosity formulation (MS/EV) and the most recent non-isotropic multiple-scale model (MS/ASM) are listed in Table 4. It can be seen that the single scale models ($k-\epsilon$ and $k-\epsilon$ /ASM) underpredict the reattachment

length while both the multi-scale models give good predictions of the reattachment length compared to the experimental data.

In terms of turbulence quantities, comparisons of the predicted streamwise and lateral turbulence intensities as well as the Reynolds stress component $\overline{uv}$ obtained from both the $k-\epsilon$ /ASM and the MS/ASM are shown in Figure 5. The results were normalized with the inlet centerline velocity. Non-isotropic turbulence structures are predicted by both models with the MS/ASM doing a better job with exceptions of near-wall regions. The inability of the models to reproduce the near-wall turbulence correctly behind the step is traced to the weakness of the wall proximate term of the pressure-strain model.

Axisymmetric Pipe Expansion Flow

The 1:3 pipe expansion flow of [14] is selected for model validations. Again, the reattachment length predictions from the four models are listed in Table 5. Both the MS models give satisfactory results. The MS/ASM actually predicted a slightly shorter reattachment length in comparison with the MS/EV model. The results of the $k-\epsilon$/ASM and the MS/ASM predictions of streamwise and radial turbulence intensities are illustrated in Figure 6. It is interesting to note that the strength of longitudinal and radial intensities (just after the pipe expansion $x/H = 2$) are very well predicted by the MS/ASM model. Within the recirculation regions, both models gave reasonable features of nonisotropic turbulence with the MS/ASM doing better performance. After the flow reattachment, the models have the tendency to predict the "return to isotropy" faster than the experiments. In the MS/ASM model, although a different turbulence time-scale is used to model this mechanism, the coefficient is not returned, i.e., the coefficient used in the conventional Rotta model is adopted without change. This aspect of modeling requires further research. The predicted turbulent shear stress from the two non-isotropic models are compared with the measurements in Figure 7. Overall, the MS/ASM model does a better job of predicting the Reynolds stress component.

CONCLUSIONS

Validation studies of the newly developed turbulence model have been presented for rotating flows, free shear flows and recirculating flows. It is evident that in general the MS models perform better than various single-scale models. The MS/ASM model also shows good capability of giving quite accurate predictions even in second order turbulence quantities for the engineering calculations. Besides, the CPU time and Computer storage for the present model are relatively inexpensive (about 20 % more for 2-D backward-facing step flows) compared to the $k-\epsilon$ model. Some discrepancies between the data and the MS/ASM solutions can be related to the pressure-strain models, especially the wall-damping model. Further validations are required to further develop the model.

ACKNOWLEDGMENTS

The authors wish to thank Alabama Super Computer for supplying CRAY time and Ms. Seema Singh for skillful typing.

NOMENCLATURE

D	jet exit diameter or width
D_{ij}	diffusion term of Reynolds stress flow
f	wall proximation function
H	step height in backward-facing step flow or expansion
k_p	turbulence kinetic energy in the production range
k_t	turbulence kinetic energy in the dissipation range
P_{ij}	production term of Reynolds stress
P_r	kinetic energy production rate
R_{ij}	Reynolds stress tensor
U_c	mean centerline velocity of jets
U_j	x_j component of mean velocity

u_j	x_j component of velocity fluctuation
x_j	coordinate direction, 1 - streamwise, 2 - transverse
x	streamwise coordinate direction
y	transverse coordinate direction
δ_{ij}	kronecker delta function
ϵ_{ij}	viscous dissipation tendor
ϵ_p	transfer rate of kinetic energy
ϵ_t	dissipation rate of kinetic energy
η	similarity coordinates
ν_t	turbulent viscosity
$\sigma_{k_p}, \sigma_{k_t}$	constants in model equations
$\sigma_{\epsilon_p}, \sigma_{\epsilon_t}$	constants in model equations
Φ_{ij}	pressure-strain tensor

REFERENCES

1. Nallasamy, M., "Turbulence Models and their Applications to the prediction of internal flows: a review", Computers & Fluids **15**, 2, 151-194 (1987).
2. Rodi, W., "Examples of Turbulence Models for Incompressible flows", AIAA J. **20**, 872 (1982).
3. Hanjalic, K. , Launder, B.E. and Schiestel R., "Multiple-Time- Scale Concepts in Turbulent Transport Modelling", in Turbulent Shear Flows 2, 36-49 (1980).
4. Kim, S.W. and Chen, C.P., "A Multiple-Time-Scale Turbulence Model Based on Variable Partitioning of Turbulent Kinetic Energy Spectrum", Numerical Heat Transfer, Part B, **16**, 193-211 (1989); Also available as NASA CR-179222 (1987).
5. Launder, B.E., "Second-Moment Closure: present... and future ? ", Int. J. Heat and Fluid Flow, **10**, 4, 282-300 (1989).
6. Launder, B.E., "Second-Moment Closure and its use in Modelling Turbulent Industrial Flows" Int. J. for Numerical Methods in Fluids, **9**, 963-985 (1989).
7. Demuren, A.O. and Rodi W., "Calculation of Turbulence-driven Secondary Motion in Non-circular Ducts", J. Fluid Mech. **140**, 189-222, (1984).
8. Mellor, G.L. and Yamada, T., " Development of a Turbulence Closure Model for Geophysical Problem", Reviews of Geophysical and spacephysics, **20**, 851 (1982).
9. Bardina, J., Ferziger, J.h. and Rogallo, R.S., "Effect of Rotation on Isotropic Turbulence: computation and modelling", J. Fluid Mech. **154**, 321-336 (1985).
10. Wigeland, R.A. and Nagib, H.M., "Grid-Generated Turbulence with and without Rotation about the streamwise direction", IIT Fluids and Heat Transfer Rep. R78-1, Illinois Inst. of Tech., Chicago, Illinois. (1978).
11. Chen, C.P. and Guo, K.L., "Similarity Solutions of Jet Flows Using a Multiple-Scale Turbulence Model", AIAA paper 89-1797 (1989).
12. Issa, R.I., "Solutions of the Implicitly Discretized Fluid Flow Equations by Operator-Splitting", J. Comp. Physics, **62**, 40, (1985).

13. Jiang, Y., Shang, H.M. and Chen, C.P., "MAST - A Multiphase All-Speed Transient Navier-Stokes Code in Generalized Coordinates", NASA CR, NAG8-092, (1990).

14. Samimy, M., Nejad, A.S. et al, "Isothermal Swirling Flow in a Damp Combuster", AIAA paper 87-1352 (1987).

15. Jones, W.P. and Launder, B.E., "The Predictions of Laminarization with a Two-Equation Model of Turbulence", Int. J. Heat and Mass Transfer **15**, 301 (1972).

16. Morse, A.P., "Axisymmetric Turbulent Shear Flows with and Without Swirl", Ph.D. Thesis, University of London, England (1977).

17. Pope, S.B., "An Explanation of the Turbulent Round Jet/ Plane Jet Anomaly", AIAA J. **16**, 279 (1978).

18. Hanjalic, K. and Launder, B.E., "Sensitizing the Dissipation Equation to Irrotational Strains", J. Fluid Eng. **102**, 39 (1980).

19. Driver, D.M. and Seegmiller, H.L., "Features of a Reattaching Turbulent Shear Layer in Divergent Channel Flow", AIAA J. **23**, 2, 163-171 (1985).

20. Robins, A., "The Structure and Development of a plane Turbulent Free jet", Ph.D. Thesis, University of London, England (1971).

21. Rodi, W., "The Prediction of Free Turbulent Boundary Layers by Use of A Two-Equation Model of Turbulence", Ph.D. Thesis, University of London, England (1972).

22. Heskestak, G., "Hot Wire Measurements in A Radial Jet", J. Appl. Mech. **88**, 417 (1966).

APPENDIX A. THE TURBULENCE MODEL CONSTANTS

Determination of the turbulence model constants is based on the assumption that the ratio k_t/k_p will asymptotically approach constant values in simple homogeneous turbulent flows such as the decay of grid turbulence, a nearly homogeneous shear flow, and the near wall equilibrium turbulent flows. The model constants also need to satisfy the realizability conditions (i.e., the turbulent kinetic energies, energy transfer rate, and dissipation rate cannot become negative). This procedure is described as following.

At hight Reynolds number, the multiple-scale model equations (1)-(4) for the homogeneous flow will be deduced as follows:

$$\frac{\partial k_p}{\partial t} = -\epsilon_p \qquad (A-1)$$

$$\frac{\partial \epsilon_p}{\partial t} = -C_{p_2}\frac{\epsilon_p^2}{k_p} - C_{p_3}\Omega\epsilon_p \qquad (A-2)$$

$$\frac{\partial k_t}{\partial t} = \epsilon_p - \epsilon_t \qquad (A-3)$$

$$\frac{\partial \epsilon_t}{\partial t} = C_{t_1}\frac{\epsilon_p\epsilon_t}{k_t} - C_{t_2}\frac{\epsilon_t^2}{k_t} - C_{t_3}\Omega\epsilon_t \qquad (A-4)$$

The above set of equations can be solved analytically. The final results are given as

$$\frac{k_p}{k_{p0}} = [1 + \frac{\epsilon_{p0}}{k_{p0}}\frac{1}{n}(\frac{1-exp(-C_{p_3}\Omega t)}{C_{p_3}\Omega})]^{-n} \qquad (A-5)$$

$$\frac{k_t}{k_{t0}} = [1 + \frac{\epsilon_{t0}}{k_{t0}}\frac{1}{m}(\frac{1-exp(-C_{t_3}\Omega t)}{C_{t_3}\Omega})]^{-m(1-\alpha)} \qquad (A-6)$$

$$\frac{\epsilon_p}{\epsilon_{p0}} = [1 + \frac{\epsilon_{p0}}{k_{p0}}\frac{1}{n}(\frac{1-exp(-C_{p_3}\Omega t)}{C_{p_3}\Omega})]^{-(n+1)}exp(-C_{p_3}\Omega t) \qquad (A-7)$$

$$\frac{\epsilon_t}{\epsilon_{t0}} = [1 + \frac{\epsilon_{t0}}{k_{t0}}\frac{1}{m}(\frac{1-exp(-C_{t_3}\Omega t)}{C_{t_3}\Omega})]^{-[m(1-\alpha)+1]}exp(-C_{t_3}\Omega t) \qquad (A-8)$$

where

$$n = \frac{1}{C_{p_2}-1}, \quad m = \frac{1}{C_{t_2}-C_{t_1}}$$

$$\alpha = \frac{\epsilon_p}{\epsilon_t} = const$$

For the grid turbulent flow without rotation, the results become

$$\frac{k_p}{k_{p0}} = (1 + \frac{t}{t_0})^{-n} \qquad (A-9)$$

$$\frac{k_t}{k_{t0}} = (1 + \frac{t}{t'_0})^{-m(1-\alpha)} \qquad (A-10)$$

$$\frac{\epsilon_p}{\epsilon_{p0}} = (1 + \frac{t}{t_0})^{-(n+1)} \qquad (A-11)$$

$$\frac{\epsilon_t}{\epsilon_{t0}} = (1 + \frac{t}{t'_0})^{-[m(1-\alpha)+1]} \qquad (A-12)$$

where

$$t_0 = n\frac{k_{p0}}{\epsilon_{p0}}, \quad t'_0 = m\frac{k_{t0}}{\epsilon_{t0}}$$

t_0 and t'_0 stand for the time scale of large eddies and small eddies, respectively. It can be seen from equation (A-9) that the value of n is the decay rate of kinetic energy k_p. According to the experimental data, $n = 1.11 \sim 1.25$, hence $C_{p_2} = 1.8 \sim 1.9$. To account for the characteristics of the energy spectrum k_t/k_p, C_{p_2} is set to be the function $1.90 \cdot (1 - 0.2 \cdot k_t/k_p + 0.2 \cdot k_t^2/k_p^2)$, In this function, the value of C_{p_2} is always within the experimental range if k_t/k_p is less or equal to one. The functional form of C_{p_2} is equivalent to the variable energy transfer function proposed by Hanjelic et al.

To recover the $k-\epsilon$ model, the constant C_{p_1} is given as conventional value 1.42. If the partition is moved to too high wave numbers, i.e., $k_t \cong 0$, then the multiple-scale model may reduce to $k-\epsilon$ model.

In order to keep the same decay rate of ϵ_p as that of ϵ_t, we set $C_{p_3} = C_{t_3}$. The value of C_{p_3} and C_{t_3} is determined as 0.042 by the computational results to fit the experimental data for homogeneous rotating flow. In this study, C_{t_3} is chosen as a function of $0.042 \cdot (1 + 0.08 \cdot \epsilon_t/\epsilon_p)$. The ratio of ϵ_t and ϵ_p is a characteristics for degree of spectral imbalance. Inclusion of ϵ_t/ϵ_p into the functional form of C_{t_3} (and C_{t_1}) allows the "inter-talk" between the large eddies and small eddies.

The values of C_{t_1} and C_{t_2} were optimized to give good agreement of the computational results with the experimental data for the free shear flows and 2D recirculating flows.

According to the observation the effect of rotation on the turbulence is to decrease the rate of dissipation of the turbulence and increase the lengthscale, especially those along the axis of rotation. Due to the generation of inertial waves, the energy transfer from large eddies to small eddies is reduced. Then the additional time scale to account for the effect of rotation is introduced in the equations of ϵ_t and ϵ_p, respectively. Ω is the angular velocity of the rotating frame and the local mean vorticity, that is defined as following form:

$$\Omega = (\Omega_{ij}\Omega_{ij})^{1/2}, \quad \Omega_{ij} = (\frac{\partial U_j}{\partial x_i} - \frac{\partial U_i}{\partial x_j})$$

Finally, it is mentioned that the prandtl numbers for turbulence quantities are set following [4], they are

$$\sigma_{k_p} = \sigma_{k_t} = 0.75, \quad \sigma_{\epsilon_p} = \sigma_{\epsilon_t} = 1.00$$

APPENDIX B. THE ALGEBRAIC STRESS MODEL FORMULATIONS

The transport equation for Reynolds stress components R_{ij} is given as

$$\frac{D}{Dt}(\rho R_{ij}) - D_{ij} = P_{ij} + \Phi_{ij} - \epsilon_{ij} \qquad (B-1)$$

in which the terms on the left hand side of equation(B-1) represent the convective and diffusive transport of R_{ij}, respectively, and the terms on the right hand side represent the production, pressure-strain and viscous dissipation tensors of Reynolds stress. Using the similitude analysis proposed by Mellor and Yamada [8], equation (B-1) can be simplified to

$$P_{ij} - \frac{2}{3}\delta_{ij}P_k + \Phi_{ij} \cong 0 \qquad (B-2)$$

The model presented in this study has the following form:

$$\Phi_{ij} = -c_1\rho\frac{\epsilon_t}{k_t}(\overline{u_iu_j} - \frac{2}{3}\delta_{ij}(k_p + k_t)) - c_2(P_{ij} - \frac{2}{3}\delta_{ij}P_k) \qquad (B-3)$$

and

$$P_{ij} = \overline{u_iu_j}\frac{\partial U_i}{\partial x_j} \qquad (B-4)$$

$$P_k = \frac{1}{2}P_{ii} \qquad (B-5)$$

Then equation (B-2) can be written as

$$P_{ij} - \frac{2}{3}\delta_{ij}P_k - c_1\rho\frac{\epsilon_t}{k_t}(\overline{u_iu_j} - \frac{2}{3}\delta_{ij}(k_p + k_t)) - c_2(P_{ij} - \frac{2}{3}\delta_{ij}P_k) = 0 \qquad (B-6)$$

or

$$(1-c_2)P_{ij} + \frac{2}{3}\delta_{ij}(c_2P_k + c_1\rho\frac{\epsilon_t}{k_t}(k_p + k_t) - P_k) = c_1\rho\frac{\epsilon_t}{k_t}\overline{u_iu_j} \qquad (B-7)$$

For 2D turbulent flow, final Reynolds stress components $\overline{u_1^2}$, $\overline{u_2^2}$, and $\overline{u_1u_2}$ were obtained as following:

$$\overline{u_1^2} = \frac{2k[\epsilon_p/3 \cdot (c_1 \cdot \epsilon_t/\epsilon_p + c_2 \cdot k_t/k - k_t/k) - k_t/k \cdot (1-c_2)\overline{u_1u_2} \cdot \partial U_1/\partial x_2]}{c_1\epsilon_t + 2k_t(1-c_2) \cdot \partial U_1/\partial x_1} \qquad (B-8)$$

$$\overline{u_2^2} = \frac{2k[\epsilon_p/3 \cdot (c_1 \cdot \epsilon_t/\epsilon_p + c_2 \cdot k_t/k - k_t/k) - k_t/k \cdot (1 - c_2)\overline{u_1 u_2} \cdot \partial U_2/\partial x_1]}{c_1\epsilon_t + 2k_t(1 - c_2) \cdot \partial U_2/\partial x_2} \qquad (B-9)$$

$$\overline{u_1 u_2} = \frac{k_t}{c_1\epsilon_t}(c_2 - 1)(\overline{u_1^2}\frac{\partial U_2}{\partial x_1} + \overline{u_2^2}\frac{\partial U_1}{\partial x_2}) \qquad (B-10)$$

where

$$k = k_p + k_t$$

APPENDIX C. WALL FUNCTION BOUNDARY CONDITIONS

To avoid the need for detailed calculations in the nearwall regions, equations are introduced to link velocities, k_p, k_t, ϵ_p, and ϵ_t on the wall to those in the logarithmic region. In this region, the flow is dominated by a one-dimensional Couette flow characterization of the flow diffusion perpendicular to the wall. Also it provides a way around this region of steep nonlinear and variation of the variable and the fact that laminar and turbulent effects become of the same order of magnitude. The new equations introduced in the momentum equations and the turbulence model equations are used in the finite difference calculations at nearwall points.

(1). **The universal velocity profile**

$$\frac{U}{U_\tau} = \frac{1}{\kappa}\ln(Ey^+) \qquad (C-1)$$

where

$$U_\tau = (\frac{\tau_w}{\rho})^{1/2} \qquad (C-2)$$

U_τ is the friction velocity; τ_w is the wall shear stress; $y^+ = yu_\tau/\nu$ is the non-dimensional wall coordinate; κ is the Von Karman constant, $\kappa = 0.4187$; E is a experimentally determined constant coefficient, $E = 9.0$.

(2). **The wall shearing stress**

Assuming τ_k is an approximation for τ_w very near the wall. The τ_k is formulated by observating that convection and diffusion of turbulence kinetic energy are nearly always negligible in this region. Deleting these terms from the k-transport equation and invoking isotropic viscosity leads to

$$\tau_k = C_\mu^{1/2}\rho k \qquad (C-3)$$

From equations (C-1) and (C-2), thus we obtained

$$\tau_w = -[\rho\kappa C_\mu^{1/4}k^{1/2}/\ln(Ey^+)]\cdot U \qquad (C-4)$$

where the negative sign is inserted since τ_w and U must have opposite directions.

(3). **The total kinetic energy**

From equation (C-2), the total kinetic energy very near the wall is given as

$$k = C_\mu^{-1/2} U_\tau^2 \qquad (C-5)$$

(4). **The energy dissipation**

As for energy dissipation near a wall, the length scale is assumed to be proportional to the normal distance from the wall, that is

$$\frac{k^{3/2}}{\epsilon} = C_l \cdot y \qquad (C-6)$$

which leads to

$$\epsilon = \frac{1}{\kappa y} C_\mu^{3/4} k^{3/2} \qquad (C-7)$$

This is the effective wall boundary condition on ϵ.

(5). **The kinetic energies k_p and k_t**

$$k = k_p + k_t \qquad (C-8)$$

If deleting convection and diffusion of turbulence kinetic energy and assuming $P_r = \epsilon_p = \epsilon_t$ in the region very near the wall , from equations (2) and (4) the ratio of k_t and k_p is derived

$$\frac{k_t}{k_p} = \frac{C_{t_1} - C_{t_2} - C_{t_3}\Omega k_t/\epsilon_t}{C_{p_1} - C_{p_2} - C_{p_3}\Omega k_p/\epsilon_p} \qquad (C-9)$$

when $\Omega \approx 0$,

$$\frac{k_t}{k_p} = \frac{C_{t_1} - C_{t_2}}{C_{p_1} - C_{p_2}} \qquad (C-10)$$

Equations (C-8) and (C-9) or (C-10) provide two constraint conditions for the kinetic energies k_p and k_t.

(6). **The Transfer rate ϵ_p and dissipation rate ϵ_t**

In the near wall region, where the turbulence is in equilibrium (the production rate is approximately equal to the dissipation rate), it can thus be assumed that

$$P_r = \epsilon_p = \epsilon_t \qquad (C-11)$$

APPENDIX D. SIMILARITY EQUATIONS FOR THE ROUND JET

The free jet flow becomes self-preserving at some distance away from its origin, similarity solutions for mean quantities and turbulence quantities exist. By proper choice of local length scale and velocity scale, the set of momentum and turbulence quantity equations can be transformed to a set of coupled non-linear ordinary differential equations. The resulting equations are quite lengthy and only the case of a round jet is summarized below.

Similarity equations for the round jet

$$-\frac{\lambda}{\eta}[f'\frac{f'}{\eta}+f(\frac{f'}{\eta})']-\frac{1}{\eta}\tau_u=\tau_u' \qquad (D-1)$$

$$-\frac{\lambda}{\eta}(2f'p+fp')=(\frac{f'}{\eta})'\tau_u-m+\frac{1}{\eta}\tau_{kp}+\tau_{kp}' \qquad (D-2)$$

$$-\frac{\lambda}{\eta}(2f'q+fq')=m-n+\frac{1}{\eta}\tau_{kt}+\tau_{kt}' \qquad (D-3)$$

$$-\frac{\lambda}{\eta}(4f'm+fm')=C_{p1}\tau_u^2\frac{m}{p}(\frac{f'}{\eta})'-C_{p2}(1-0.2\frac{q}{p}+0.2\frac{q^2}{p^2})\frac{m^2}{p}$$
$$-C_{p3}m[\lambda^2\eta f''+(\frac{f'}{\eta})']+\frac{1}{\eta}\tau_{\epsilon p} \qquad (D-4)$$

$$-\frac{\lambda}{\eta}(4f'n+fn')=C_{t1}(1+0.01\frac{n}{m})\frac{mn}{q}-C_{t2}\frac{n^2}{q}$$
$$-C_{t3}(1+0.08\frac{n}{m})n[\lambda^2\eta f''+(\frac{f'}{\eta})']+\frac{1}{\eta}\tau_{\epsilon t} \qquad (D-5)$$

$$\lambda'=0 \qquad (D-6)$$

Boundary conditions:

$$\text{at}\quad \eta=0:\quad \frac{f'}{\eta}=1;\ f=p'=q'=m'=n'=f''=0 \qquad (D-7)$$

$$\text{at}\quad \eta=1:\quad m'=0;\ p=q=m=n=0 \qquad (D-8)$$

Definition of variables:

$$()'=\frac{d}{d\eta},\quad l(x_1)=\lambda x_1,\quad \tilde{\nu_t}=C_\mu\frac{(p+q)^2}{m},$$

$$p = \frac{k_p}{U_c^2}, \quad q = \frac{k_t}{U_c^2}, \quad m = \frac{\epsilon_p l(x_1)}{U_c^3}, \quad n = \frac{\epsilon_t l(x_1)}{U_c^3},$$

$$\eta = \frac{x_2}{l(x_1)}, \quad \frac{U_1}{U_c} = \frac{f'}{\eta}, \quad \tau_u = \tilde{\nu}_t \left(\frac{f'}{\eta}\right)',$$

$$\tau_{kp} = \frac{\tilde{\nu}_t}{\sigma_{kp}} p', \quad \tau_{kt} = \frac{\tilde{\nu}_t}{\sigma_{kt}} q', \quad \tau_{\epsilon p} = \frac{\tilde{\nu}_t}{\sigma_{\epsilon p}} m', \quad \tau_{\epsilon t} = \frac{\tilde{\nu}_t}{\sigma_{\epsilon t}} n'.$$

It would suffice to say that due to the complete neglect of molecular diffusion, the choice of the characteristic length scale corresponds to the locus of points where the turbulent diffusivities are zero. The location of these points must be calculated as part of the solution to the problem. The existence of this sharp boundary is insured by requiring the turbulent diffusivity (ν_t) to be zero there.

TABLE 1

Constants and Functions of Multiple-Scale Model

Constant or Function	Value or form
C_{P_1}	1.42
C_{P_2}	$1.90(1 - 0.2k_t/k_p + 0.2k_t^2/k_p^2)$
C_{P_3}	0.042
C_{t_1}	$0.96(1 + 0.01\epsilon_t/\epsilon_p)$
C_{t_2}	1.12
C_{t_3}	$0.042(1 + 0.08\epsilon_t/\epsilon_p)$
σ_{k_p}	0.75
σ_{k_t}	0.75
σ_{ϵ_p}	1.00
σ_{ϵ_t}	1.00

TABLE 2

Experimental data of Wigeland and Nagib (1978) at initial time (Ut/m=20) and parameter ranges covered

Case (1): $M = 0.0039$ (m)			
Ω (s^{-1})	0	20	80
U (m/s)	8.69	8.66	8.82
U_s (m/s)	8.69	8.67	8.96
k (m^2/s^2)	0.10625	0.10105	0.1157
ϵ (m^2/s^3)	17.67	16.45	18.19
Case (2): $M = 0.00625$ (m)			
Ω (s^{-1})	0	20	80
U (m/s)	5.33	5.45	5.48
U_s (m/s)	5.33	5.46	5.71
k (m^2/s^2)	0.0425	0.0453	0.04975
ϵ (m^2/s^3)	2.649	3.591	3.300
Case (3): $M = 0.00254$ (m)			
Ω (s^{-1})	0	20	80
U (m/s)	8.51	8.58	8.79
U_s (m/s)	8.51	8.59	8.93
k (m^2/s^2)	0.0885	0.0887	0.09845
ϵ (m^2/s^3)	24.27	22.56	22.42

TABLE 3

Spreading Rate Predictions Versus Experiments

Model	Plane Jet	Round Jet	Radial Jet
$k-\epsilon$ [3]	0.110	0.125	0.094
Morese [5]	0.102	0.085	0.099
Pope [2]	0.110	0.091	0.042
Hanjalic & Launder [6]	0.119	0.107	0.077
Chen & Guo	0.111	0.084	0.094
Experiment	0.100 - 0.110	0.086 - 0.09	0.098 - 0.110

TABLE 4

Reattachment length for Backward facing step turbulent flows

9:1 Experiment Driver and Seegmiller(1986)

Experiment	$k-\epsilon$	Multiple-Scale	$k-\epsilon$/ ASM	MS / ASM
~ 6.1	4.76	5.94	4.65	5.70

TABLE 5

Reattachment length for Axissymatrical Recirculating turbulent flows

3:1(Axis.) Experiment Najed(1987)

Experiment	$k-\epsilon$	Multiple-Scale	$k-\epsilon$/ ASM	MS / ASM
~ 9	7.10	8.82	6.80	8.70

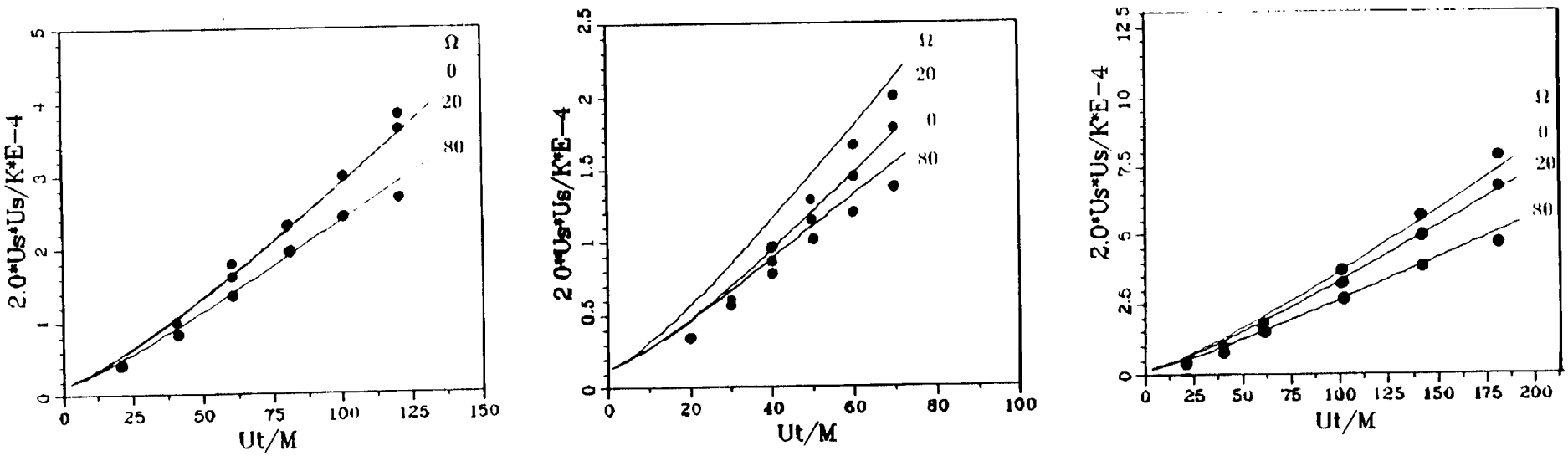

Figure. 1 Predictions of Wigeland and Nagib's data on the decay of homogeneous rotating turbulent Flow

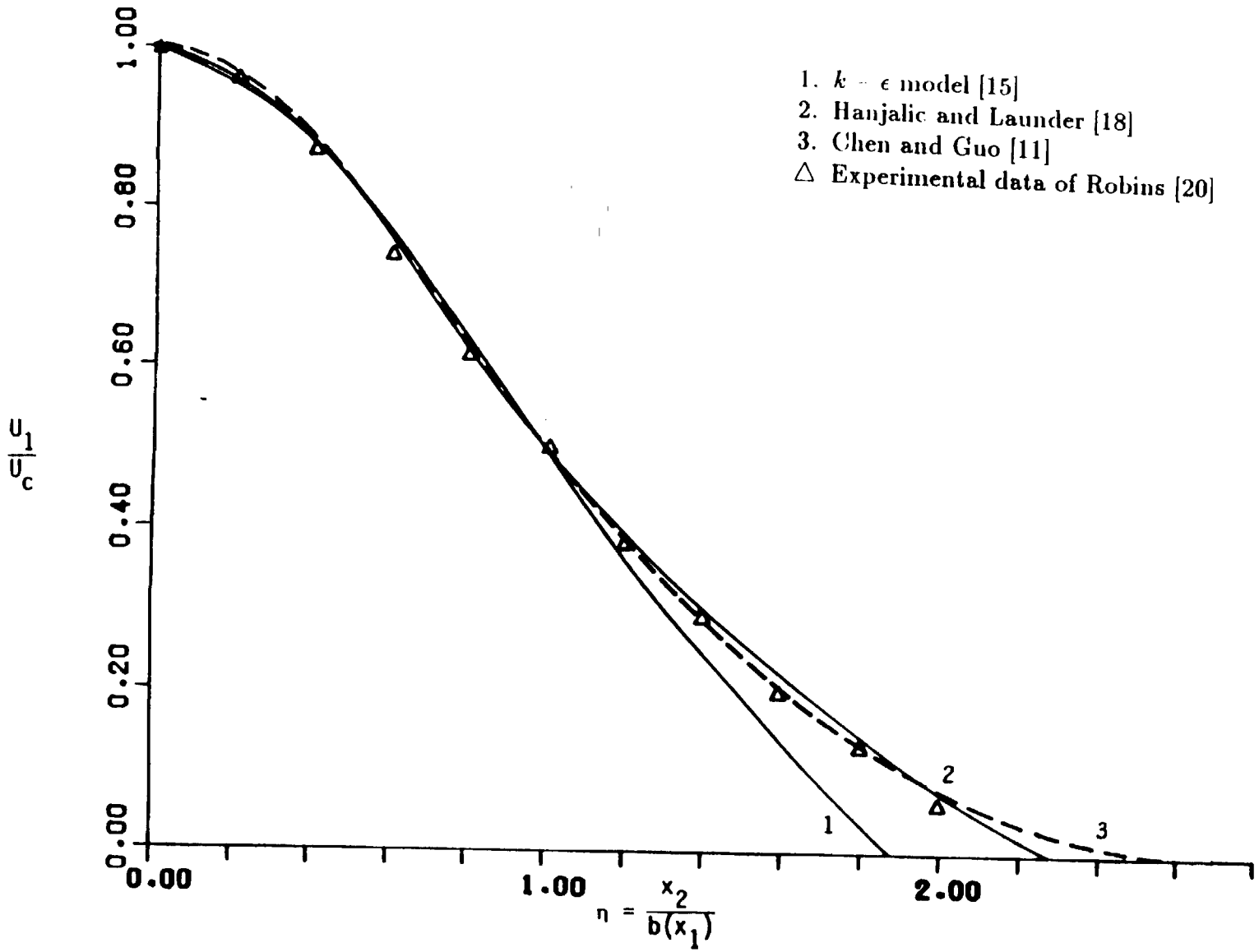

Figure. 2 Comparision of computational and experimental mean velocity for the plane jet

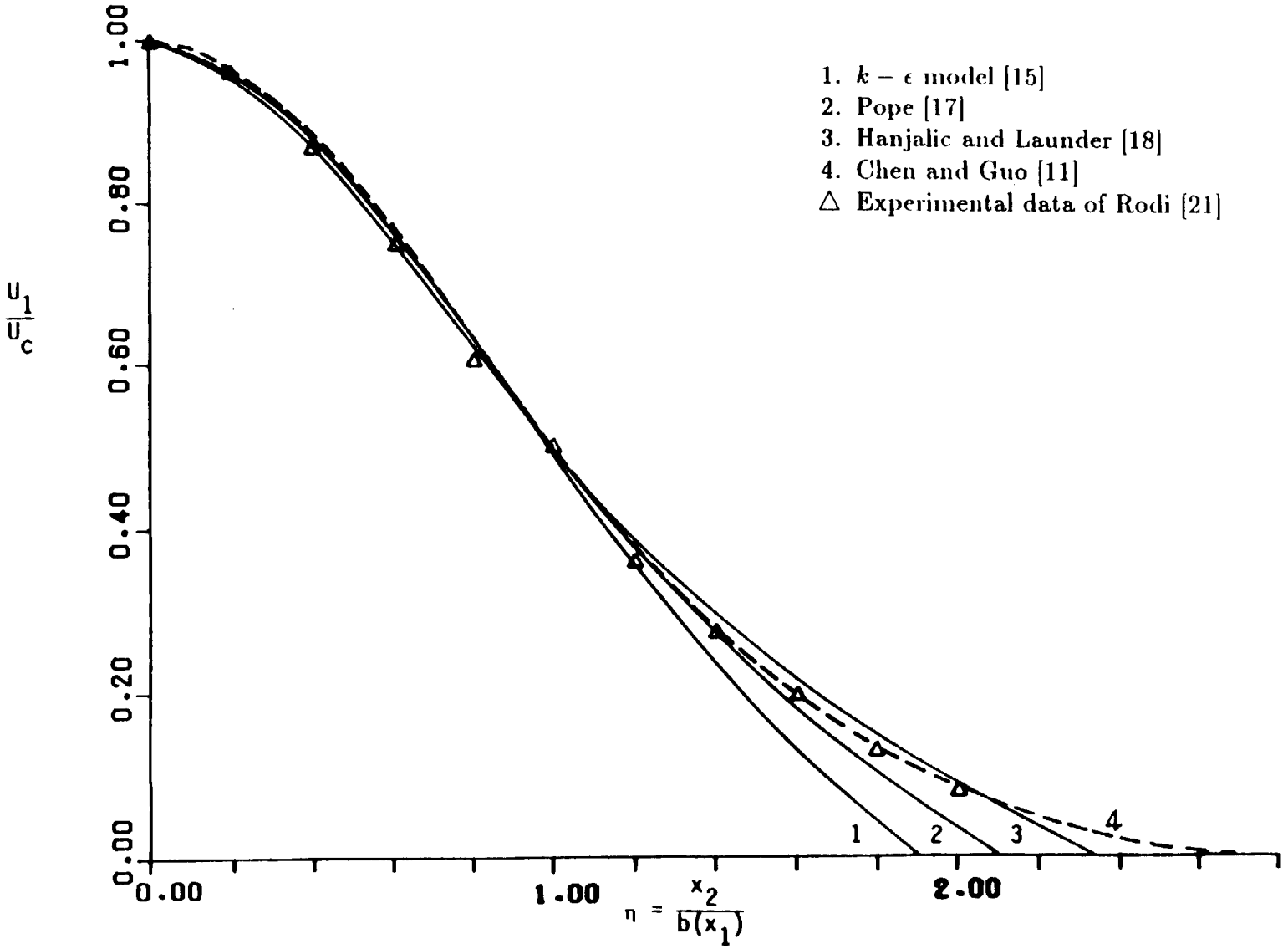

Figure. 3 Comparision of computational and experimental mean velocity for the round jet

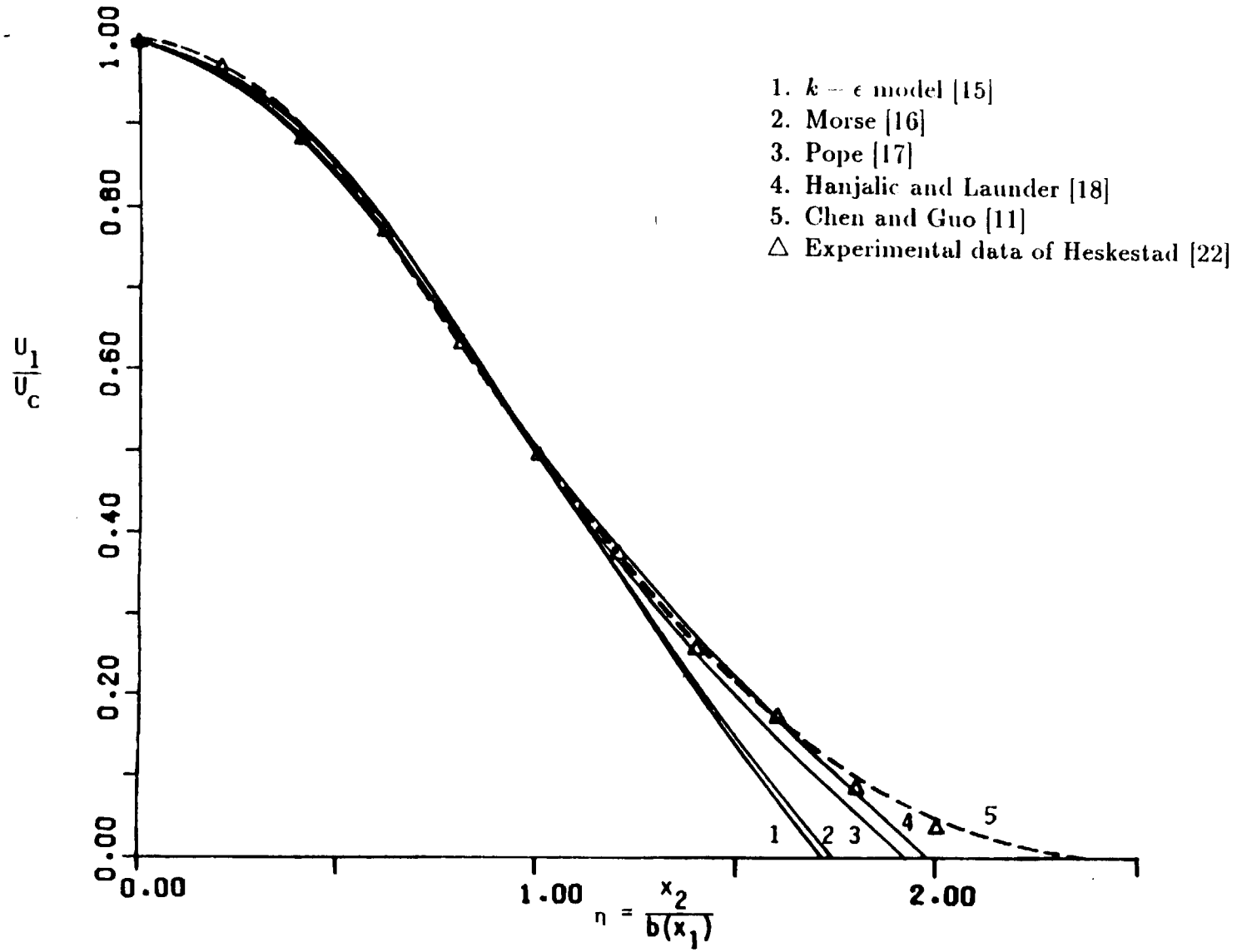

Figure. 4 Comparision of computational and experimental mean velocity for the radial jet

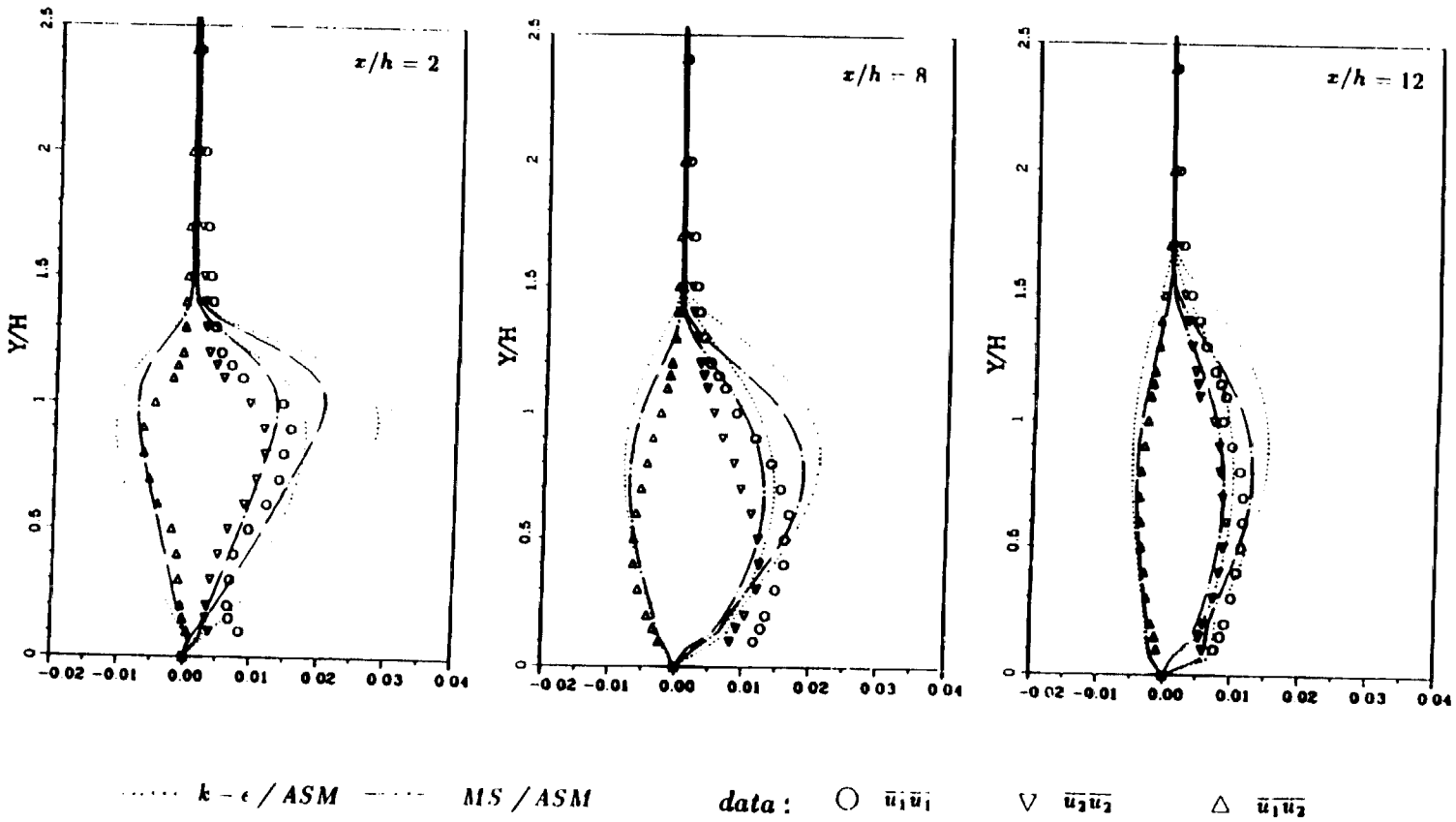

Figure. 5 Reynolds stresses profiles for the backward facing step turbulent flow (9:1)

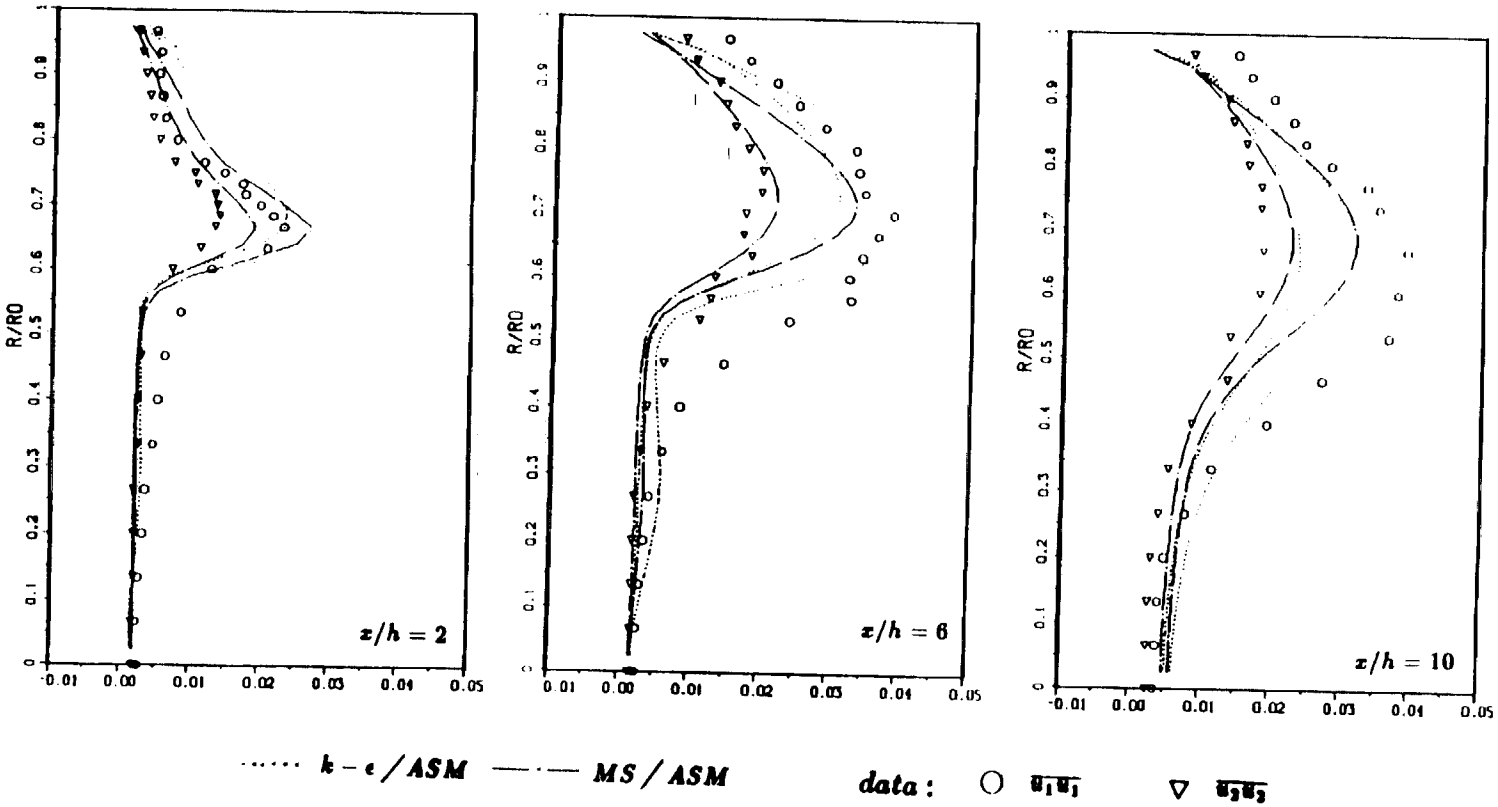

Figure. 6 Axial and radial turbulence intensities profiles for the recirculating turbulent flow (3:1, Axis.)

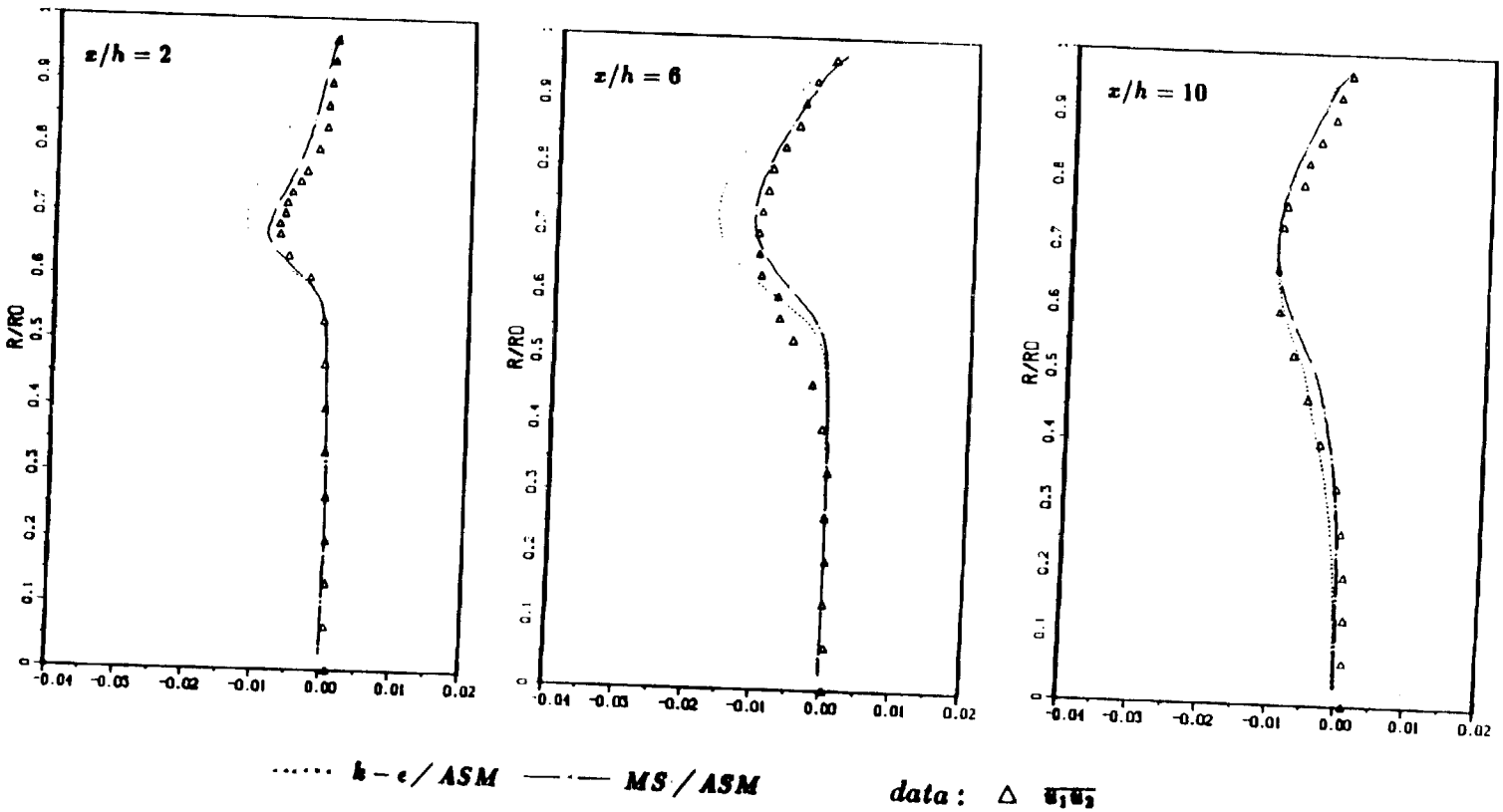

Figure. 7 Reynolds stress profiles for the recirculating turbulent flow (3:1, Axis.)

319213
P.38

NASA
National Aeronautics and Space Administration

Report Documentation Page

1. Report No.	2. Government Accession No.	3. Recipient's Catalog No.

4. Title and Subtitle	5. Report Date
Turbulence Modeling-Computational Dynamics	September 15, 1990
	6. Performing Organization Code: U. A. H.

7. Author(s)	8. Performing Organization Report No.
Dr. C. P. Chen	10. Work Unit No.

9. Performing Organization Name and Address	11. Contract or Grant No.
The University of Alabama in Huntsville Huntsvile, AL 35899	NAS8-36955 D.O. 31
	13. Type of Report and Period Covered: Final Report

12. Sponsoring Agency Name and Address	14. Sponsoring Agency Code
NASA-Marshall Space Flight Center MSFC, AL 35812	

15. Supplementary Notes

16. Abstract

This report describes a newly developed non-isotropic multiple-scale turbulence model (MS/ASM) for complex flow calculations. This model focuses on the direct modeling of Reynolds stresses and utilizes split-spectrum concepts for modeling multiple-scale effects in turbulence. Validation studies on free shear flows, rotating flows and recirculating flows show that the current model perform significantly better than the single-scale k-ε model. The present model is relatively inexpensive in terms of CPU time which makes it suitable for broad engineering flow applications.

17. Key Words (Suggested by Author(s))	18. Distribution Statement
Non-isotropic Model Multiple-scale Model	

19. Security Classif. (of this report)	20. Security Classif. (of this page)	21. No. of pages	22. Price
Unclassified	Unclassified	36	

NASA FORM 1626 OCT 86